Earth and Planetary Science Letters 357–358 (2012) 355–365

Contents lists available at SciVerse ScienceDirect

Earth and Planetary Science Letters

journal homepage: www.elsevier.com/locate/epsl

Oxygen isotopes in crystalline silicates of comet Wild 2: A comparison of oxygen isotope systematics between Wild 2 particles and chondritic materials

Daisuke Nakashima [a,*], Takayuki Ushikubo [a], David J. Joswiak [b], Donald E. Brownlee [b], Graciela Matrajt [b], Michael K. Weisberg [c,d], Michael E. Zolensky [e], Noriko T. Kita [a]

[a] WiscSIMS, Department of Geoscience, University of Wisconsin-Madison, Madison, WI 53706, USA
[b] Department of Astronomy, University of Washington, Seattle WA 98195, USA.
[c] Department of Physical Sciences, Kingsborough Community College and Graduate Center, City University of New York, Brooklyn, NY 11235, USA.
[d] Department of Earth and Planetary Sciences, American Museum of Natural History, New York, NY 10024, USA.
[e] Astromaterials Research and Exploration Science, NASA Johnson Space Center, Houston, TX 77058, USA

ARTICLE INFO

Article history:
Received 9 May 2012
Received in revised form
19 September 2012
Accepted 24 September 2012
Editor: Dr. B. Marty
Available online 26 October 2012

Keywords:
oxygen isotope ratios
crystalline silicate
comet 81P/Wild 2
solar system formation
Stardust

Abstract: Oxygen three-isotope ratios of nine crystalline silicate particles from comet Wild 2 were measured to investigate oxygen isotope systematics of cometary materials. We are able to analyze particles as small as 4 μm using an ion microprobe with a $\sim 1 \times 2$ μm beam by locating the analysis spots with an accuracy of ± 0.4 μm. Three particles of Mn-rich forsterite, known as low-iron, manganese-enriched (LIME) olivine, showed extremely ^{16}O-rich signatures (δ^{18}O, δ^{17}O ~ -50‰), similar to refractory inclusions in chondrites. The three Mn-rich forsterite particles may have formed by condensation from an ^{16}O-rich solar nebula gas. Other particles consist of olivine and/or pyroxene with a wide range of Mg# [=molar MgO/(FeO+MgO) %] from 60 to 96. Their oxygen isotope ratios plot nearly along the carbonaceous chondrite anhydrous mineral (CCAM) and Young and Russell lines with $\Delta^{17}O(=\delta^{17}O-0.52\times\delta^{18}O)$ values of −3.0‰ to +2.5‰. These data are similar to the range observed from previous analyses of Wild 2 crystalline silicates and those of chondrules in carbonaceous chondrites. Six particles extracted from Stardust track 77 show diverse chemical compositions and isotope ratios; two Mn-rich forsterites, FeO-poor pigeonite, and three FeO-rich olivines with a wide range of Δ^{17}O values from −24‰ to +1.6‰. These results confirmed that the original projectile that formed track 77 was an aggregate (>6 μm) of silicate particles that formed in various environments.

The Δ^{17}O values of ferromagnesian Wild 2 particles (including data from previous studies) increase from ~−23‰ to +2.5‰ with decreasing Mg#: Δ^{17}O values of Mn-rich forsterite particles (Mg#=98–99.8) cluster at −23‰, those of FeO-poor particles (Mg#=95–97) cluster at −2‰, and those of FeO-rich particles (Mg# ≤ 90) scatter mainly from −1.5‰ to +2.5‰. Compared to chondrules in primitive chondrites, the systematic trend between Mg# and Δ^{17}O among the Wild 2 particles is most similar to that reported for CR chondrite chondrules. We argue that CR chondrites and some cometary materials share multiple common chemical and isotope characteristics. We suggest that many of the crystalline silicate particles formed in the outer regions of the asteroid belt, or regions that share the common properties, and were transported to comet-forming regions and accreted into comet Wild 2.

1. Introduction

Short-period comets are ancient bodies of ice and silicate that accreted in cold regions of the solar nebula and are now located in the Kuiper belt. Returned samples from short-period comet 81P/Wild 2 (Stardust Mission; Brownlee et al., 2006) were expected to contain primitive Solar system materials, in particular similar to those in anhydrous chondritic porous interplanetary dust particles (commonly referred as CP IDPs), most of which are believed to be cometary in origin (cf., Bradley, 2003). The abundance of presolar grains in Wild 2 is on the order of 1000 ppm (Leitner et al., 2012; see also Messenger et al., 2009), which overlaps with the range observed in primitive IDPs (~400 ppm and sometimes even up to %-range; Floss et al., 2006; Busemann et al., 2009). GEMS (glass with embedded metal and sulfide) grains and enstatite whiskers, which are notable silicate materials in anhydrous porous IDPs, were not found, because they may have been destroyed during capture (Ishii et al., 2008). Recently, Stodolna

* Corresponding author. Tel.: +1 608 261 1523; fax: +1 608 262 0693.
E-mail address: naka@geology.wisc.edu (D. Nakashima).

0012-821X/$ - see front matter © 2012 Elsevier B.V. All rights reserved.
http://dx.doi.org/10.1016/j.epsl.2012.09.041

et al. (2012) identified an enstatite whisker in a Wild 2 particle. Crystalline silicate particles from Wild 2 that resemble Ca–Al-rich inclusions (CAIs) and chondrules in chondrites were discovered (McKeegan et al., 2006; Zolensky et al., 2006; Nakamura et al., 2008, 2009; Ishii et al., 2010; Bridges et al., 2012; Joswiak et al., 2012; Ogliore et al., 2012). The discoveries of high temperature solids (~2000 K) are surprising, because it has been expected that silicates in comets would be dominated by amorphous or annealed nanocrystalline solids (~1000 K) (cf., Brownlee et al., 2012), but these were not found. Ciesla (2007), among others, suggested radial transport of the high temperature solids from the inner to the outer solar nebula regions and capture by accreting cometary objects to explain the presence of chondrule- and CAI-like objects in Wild 2. Some studies suggested that parent asteroids of carbonaceous chondrites may represent cometary materials that were implanted into the asteroid belt (e.g., Lodders and Osborne, 1999; Gounelle et al., 2008).

Previous studies of crystalline silicates from Wild 2 showed heterogeneous oxygen isotope ratios from −50‰ to ~0‰ in both $\delta^{18}O$ and $\delta^{17}O$ values (deviation of $^{18}O/^{16}O$ and $^{17}O/^{16}O$ ratios from Standard Mean Ocean Water in parts per thousands, known as SMOW-scale). The most ^{16}O-rich data are obtained from the CAI-like particle Inti (track 25; McKeegan et al., 2006), a relict olivine grain in the chondrule-like particle Gozen-sama (track 35; Nakamura et al., 2008), and an olivine particle (track 112; Nakamura-Messenger et al., 2011). Other Wild 2 particles are ^{16}O-poor with $\Delta^{17}O(=\delta^{17}O-0.52\times\delta^{18}O)$ values mainly ranging from −5‰ to +1‰ (McKeegan et al., 2006; Nakamura et al., 2008; Nakashima et al., 2011a; Bridges et al., 2012; Ogliore et al., 2012), covering a range similar to those of anhydrous IDPs, and suggesting a genetic link between the Wild 2 particles and anhydrous IDPs (Aléon et al., 2009; Nakashima et al., 2011a, 2012). Many of these ^{16}O-poor crystalline silicates from Wild 2 particles show mineral compositions and petrographic textures similar to those in chondrules (e.g., Nakamura et al., 2008). Thus, it is important to compare oxygen isotope data from Wild 2 particles with those in chondrules in primitive chondrites (e.g., Krot et al., 2006a).

Recently, high precision SIMS analyses of minerals and glass in more than 40 chondrules from Acfer 094 (ungrouped C3.0) revealed that the oxygen isotope ratios of individual chondrules are internally homogeneous, except for relatively minor relict olivine grains, and represent the oxygen isotope reservoirs of the local protoplanetary disk (Ushikubo et al., 2012). Furthermore, chondrules in Acfer 094 show the bimodal $\Delta^{17}O$ values at −5‰ and −2‰ that negatively correlate with the Mg# [=molar MgO/(MgO+FeO) %] of phenocrysts, which suggests the existence of two separated isotope reservoirs with different redox states. Other primitive (≤3.0) carbonaceous chondrites also show a similar systematic trend between Mg# and $\Delta^{17}O$ values, though the detail trends are specific to individual chondrite groups (e.g., Connolly and Huss, 2010; Nakashima et al., 2010; Tenner et al., 2011a, 2011b, 2012; Schrader et al., 2012). Ushikubo et al. (2012) also pointed out that the oxygen isotope ratios of chondrule-like objects studied by Nakamura et al. (2008) match the isotope reservoirs with $\Delta^{17}O$ value of −2‰, which would widely distribute throughout the outer solar system. The total number of Wild 2 particles that were analyzed for oxygen isotopes with sufficient precision (±1−2‰; 2σ and 2SD) is still limited (n=10; McKeegan et al., 2006; Nakamura et al., 2008, 2009; Nakashima et al., 2011a; Ogliore et al., 2012). Detailed mineral chemistry data of these particles are not always available. Therefore, the detailed distributions of $\Delta^{17}O$ and Mg# values among Wild 2 particles are not well known.

Among the Wild 2 crystalline silicates, Mn-rich forsterite, also known as low-iron, manganese-enriched (LIME) olivine, has been identified in Stardust tracks (Zolensky et al., 2006; Joswiak et al., 2012), although no oxygen isotope analyses have been obtained so far. LIME olivine was originally found in IDPs and primitive chondrites (e.g., Klöck et al., 1989; Weisberg et al., 2004). Ebel et al. (2012) suggested that LIME olivine was a condensate from a vapor of solar composition (see also Klöck et al., 1989). Oxygen isotope analyses of LIME olivine from an IDP showed an ^{16}O-poor signature ($\Delta^{17}O=-2$‰; Aléon et al., 2009) similar to other anhydrous IDPs, while those in AOAs from CR2 chondrites show ^{16}O-rich signatures ($\Delta^{17}O\sim-20$‰; Weisberg et al., 2007), indicating there could be various formation processes/environments for LIME olivine.

In this study, we analyzed the oxygen isotope ratios of nine ferromagnesian Wild 2 particles in order to compare them to chondrules in various types of primitive chondrites. We report analyses of six particles from a single Stardust track (track 77) with a wide range of Mg# (Joswiak et al., 2012), which allow us to explore the diversity of oxygen isotope ratios within the original Wild 2 projectile. Three Mn-rich forsterites were also selected for the study, two from track 77 and one from track 57; we report the oxygen isotope ratios of LIME olivine from Wild 2 particles for the first time.

We established routine analyses of tiny particles (≤10 μm in diameter) at 1–2‰ precision using the IMS-1280 ion probe at the WiscSIMS laboratory (Nakamura et al., 2008; Nakashima et al., 2011b). In this study, we applied two modifications to the established analytical procedures for more accurate analyses: (1) use of indium to mount microtomed samples which avoids the risk of consuming a significant portion of the samples during repolishing to re-expose the microtomed surface and (2) use of focused ion beam (FIB) marking on the sample surface that is identified by the $^{16}O^-$ secondary ion imaging for improving aiming accuracy.

2. Analytical procedures

2.1. Sample preparation

The accuracy of oxygen isotope analyses using a secondary ion mass spectrometer (SIMS or ion microprobe) depends on the topography of the sample surface from which secondary ions are generated (Kita et al., 2009). In the previous studies, particles with microtomed surfaces were individually embedded in epoxy resin along with a mineral standard, which were then ground and polished to flat disks with a 6–8 mm radius (Nakamura et al., 2008; Nakashima et al., 2012). These small epoxy disks were suitable for accurate oxygen isotope analyses in terms of minimal sample topography and hydride production (Nakashima et al., 2011b). One of the Wild 2 particles in this study was prepared using an 8 mm epoxy disk, the same mounting technique of Nakashima et al. (2011b, 2012). However, the procedure of mounting small particles (≤10 μm) is difficult and there is a risk of consuming a significant portion of the remaining samples during repolishing. For the remaining 8 particles in this study, we used acrylic cubes (~100 μm) containing particles with microtomed surfaces that were pressed into indium in 8 mm aluminum disks, without reprocessing the surface. Polished San Carlos olivine standard grains (~100–200 μm in size) were also mounted into the disks. Detailed procedures for sample mounting methods are described in the Supplementary information.

In each mount, the Wild 2 particle and San Carlos olivine standard were positioned within a 0.7 mm-radius from the center of the aluminum disk in order to minimize the instrumental mass fractionation between samples and standards (≤ ±0.5‰ in $\delta^{18}O$ within 1 mm-radius of the 8 mm disks; Nakashima et al., 2011b). The flatness of the sample mounts using indium was examined by a ZYGO NewView white light profilometer at the Materials

Science Center, University of Wisconsin. The flatness of the entire aluminum disk including indium, acrylic cube, sample particle, and San Carlos olivine was typically within 5 μm.

2.2. Electron microscopy

Backscattered electron (BSE) and secondary electron (SE) images of the Wild 2 particles were obtained using field emission scanning electron microscopes (FE-SEMs) and a SEM at several steps of sample preparation including: before mounting in aluminum disks, after FIB marking, and after oxygen isotope analyses. Periods of exposure of samples to the electron beam were minimized so as to avoid significant depressions or deformation of acrylic (and epoxy) surrounding the Wild 2 particles, because the topography or tilting of the sample surface could cause a significant instrumental mass fractionation in oxygen isotope ratios (Kita et al., 2009).

Major element compositions of microtomed thin sections of the Wild 2 particles were obtained using a FEI TF20 scanning transmission electron microscope equipped with an energy-dispersive X-ray spectrometer (TEM-EDS), for which measurement parameters were described in Joswiak et al. (2009). The chemical compositions were reported in Matrajt et al. (2008) and Joswiak et al. (2009, 2012). Elemental compositions of a particle in an epoxy mount were measured with an electron probe microanalyzer (EPMA; CAMECA SX100) equipped with five wavelength-dispersive X-ray spectrometers (WDS) at the American Museum of Natural History. WDS quantitative chemical analyses of individual silicate phases were performed at 15 kV accelerating voltage and 15 nA beam current with a focused beam of approximately 1 μm in diameter.

2.3. FIB marking and sample aiming

In the previous studies, the accuracy of aiming the analysis locations was limited by the optical resolution of the reflected light microscope (originally ~3.5 μm, but recently improved to 1.8 μm using a UV light source). Inaccurate aiming causes significant beam overlap with surrounding resin and adjacent mineral phases and aerogel, which results in inaccurate oxygen isotope ratios. In the present study, we employed FIB marking at the selected locations of each sample prior to the ion microprobe analyses, which were identified by the $^{16}O^-$ secondary ion imaging. A Zeiss 1500XB CrossBeam workstation equipped with a gallium ion source at the University of Wisconsin was used to remove surface coatings from the Wild 2 particles (carbon and palladium coatings ~40 nm) and a San Carlos olivine standard for test analyses (carbon coating ~20 nm; see the Supplementary information). A 30 keV focused Ga^+ ion beam set to 2–5 pA was rastered within a 1 μm × 1 μm square on the sample surface for ~90–100 s, so that only the surface coating was removed without significant milling of silicate mineral from the sample surface (Fig. 1a). For smaller particles (less than 4 μm of surface exposure), only one FIB square was made at the center. For larger particles ($\geq$4 μm) two FIB squares were made on the surface guided by BSE images of the same particles.

Prior to each oxygen isotope analysis, secondary $^{16}O^-$ ion images of the Wild 2 particles with FIB squares were obtained using the CAMECA IMS-1280 ion microprobe at the University of Wisconsin (WiscSIMS; Kita et al., 2009). The Cs^+ ion beam was focused to $\leq$1 μm diameter (~1 pA) that was rastered over an area of 10 μm × 10 μm. The secondary $^{16}O^-$ ions were detected with a multi-collector electron multiplier (EM; L2) by applying an X-deflector after the secondary magnet (DSP2X) without moving other multi-collection detectors nor changing the magnetic field that was set up for the oxygen isotope analysis. Since the carbon and palladium coatings of the 1 μm × 1 μm square within the Wild 2 particles were previously removed using FIB, the $^{16}O^-$ signals were generated only from the FIB square within 5 min of sputtering (Fig. 1b). The intensity of the primary beam used for ion imaging was low enough that the rest of surface coating remained intact. Following this, we moved the stage in order to

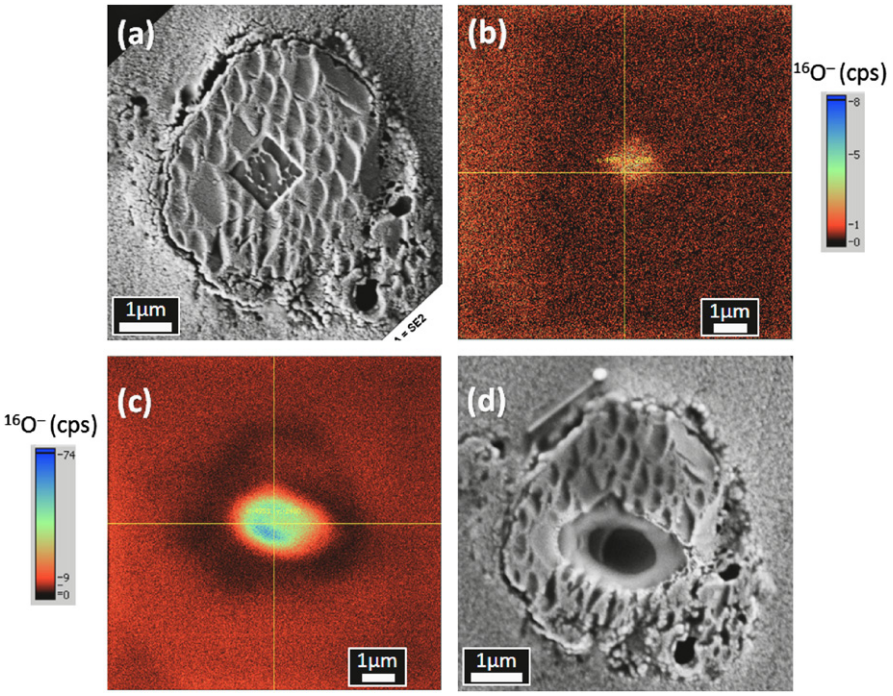

Fig. 1. An SE image of a Wild 2 particle (fragment 4 from track 77) after FIB marking (a), an $^{16}O^-$ ion image (10 μm × 10 μm) of the Wild 2 particle before the oxygen isotope analysis (b), an $^{16}O^-$ ion image (10 μm × 10 μm) of the Wild 2 particle after the oxygen isotope analysis (c), and an SE image of the Wild 2 particle after the oxygen isotope analysis (d). In panels a and d, irregular surface with many dimples of the Wild 2 particle was made by microtoming to obtain TEM thin sections. In panels b and c, centers of cross-wires correspond to the center of the Cs^+ primary beam. The $^{16}O^-$ ion images were taken in 512 × 512 pixels (~20 nm/pixel) and in linear scale.

locate the FIB square to the center of the 10 μm × 10 μm raster area where the oxygen three-isotope analysis was made in spot mode as described below. The 10 μm × 10 μm $^{16}O^-$ ion images were taken after each SIMS analysis to confirm the positions of analyzed spots (Fig. 1c). The new aiming protocol is applied for the particles smaller than ~10 μm in size. We confirmed that there was no detectable instrumental mass fractionation on the FIB squares through the test analyses on a San Carlos olivine grain (see the Supplementary information).

2.4. Oxygen isotope analyses

Oxygen isotope ratios of the nine Wild 2 particles were analyzed with the WiscSIMS IMS-1280. The analytical conditions and measurement procedures were similar to those in Nakashima et al. (2011b, 2012). The 8 mm aluminum (or epoxy) disks containing the Wild 2 particles were mounted in the sample holding disk (25 mm in diameter) with three holes (8 mm in diameter), which minimized the surface topography effects on high precision SIMS stable isotope analyses of cometary particles (Nakashima et al., 2011b). A focused Cs^+ primary beam was set to ~1 μm × 2 μm and intensity of ~3 pA. The secondary $^{16}O^-$, $^{17}O^-$, and $^{18}O^-$ ions were detected simultaneously by a Faraday Cup ($^{16}O^-$) and electron multipliers ($^{17}O^-$, $^{18}O^-$) on the multi-collection system. Intensities of $^{16}O^-$ were ~1 – 2 × 10^6 cps. The contribution of the tailing of $^{16}O^1H^-$ interference to $^{17}O^-$ signal was corrected by the method described in Heck et al. (2010), though the contribution was negligibly small (≤ 0.4‰). Nine particles were analyzed in three separate sessions (see the Supplementary Table A1).

One to five analyses were performed for each Wild 2 particle, bracketed by eight to nine analyses (four or five analyses before and after the unknown sample analyses) on the San Carlos olivine grains mounted in the same disks. For one mount, the San Carlos olivine standard grain in the same aluminum disk was not used as a running standard, because the standard grain showed irregular surface and was not suitable for standardization. Instead, a San Carlos olivine grain mounted in other hole was used for standardization, where an inter-hole instrumental mass bias does not change more than 0.5 – 0.7‰ in $\delta^{18}O$ (Nakashima et al., 2011b). The external reproducibility of the running standards was 1.4 – 3.0‰ for $\delta^{18}O$, 1.0–2.8‰ for $\delta^{17}O$, and 1.2 – 2.5‰ for $\Delta^{17}O$ (2SD; standard deviation), which were assigned as analytical uncertainties of unknown samples (see Kita et al., 2009, 2010 for detailed explanations). We analyzed two olivine (Fo_{100} and Fo_{60}), two low-Ca pyroxene (En_{97} and En_{85}), diopside, and plagioclase (An_{60}) standards (Valley and Kita, 2009; Kita et al., 2010) in the same session for correction of instrumental bias of olivine, pyroxene, and plagioclase. Instrumental biases estimated from above mineral standards (matrix effect) are within a few ‰ in $\delta^{18}O$ (Supplementary Table A2; see also Valley and Kita, 2009; Ushikubo et al., 2012). After SIMS analyses, all SIMS pits were inspected using a FE-SEM to confirm the analyzed positions (Fig. 1d).

3. Sample description

Nine ferromagnesian crystalline silicate Wild 2 particles (Fig. 2) were selected for the oxygen isotope study from four Stardust tracks (cf., Joswiak et al., 2009, 2012) including one particle from track 22 (track name Aton), one particle from track 57 (track name Febo), six particles from track 77 (track name Puki), and one particle from track 81. These particles were chosen in part according to the availability of particles large enough for one to multiple spot analyses, as well as with the purpose of examination of multiple grains in track 77 that are known to contain particles with a wide range of chemistry (Joswiak et al., 2009, 2012).

3.1. Particles from track 77

Track 77 (T77) is a type B track (Burchell et al., 2008), which has a broad cavity near the entry point and ends in three prominent separate terminal grains, one being by far the largest (Joswiak et al., 2012). It was suggested that the original projectile was a loose aggregate (> 6 μm in diameter) of mineral grains and disruption of the aggregate may have formed the broad cavity near the entry point during impact into aerogel (Joswiak et al., 2009, 2012). Particles from T77 were classified as coarse-grained particles if they were larger than ~1 μm (Joswiak et al., 2012). Six T77 particles analyzed in this study consist of single (or multiple) minerals larger than 1 μm. Fragments 1 (terminal particle), 5, and 50 were each mounted in separate aluminum disks, while fragments 4, 6, and 9 were mounted in a single aluminum disk. Two particles consist of FeO-rich olivine: fragment 1 (hereafter F1/T77; Fo_{62-67}; Fig. 2a) and fragment 4 (hereafter F4/T77; Fo_{58-61}; Fig. 2b) (Joswiak et al., 2012). Two particles consist of forsterite: fragment 6 (hereafter F6/T77; $Fo_{99.8}$; Fig. 2d) and fragment 50 (hereafter F50/T77; $Fo_{99.8}$; Fig. 2f). F6/T77 and F50/T77 contain MnO of 0.35 and 0.46 wt% and FeO of 0.11 wt% and 0.18 wt%, respectively. Because the MnO/FeO ratios are > 1, the two particles are classified as LIME olivines (cf., Klöck et al., 1989). In fragment 5 (hereafter F5/T77; Fig. 2c), FeO-rich olivine (Fo_{66}), Na- and Cr-bearing diopside ($En_{42}Wo_{46}$; kosmochloric pyroxene), and Al–Si-glass are intimately mixed (Joswiak et al., 2012). Such mineral assemblages (Kool grains) are observed only in other Stardust tracks and IDPs and have chemical compositions similar to those of type II chondrules in ordinary chondrites (Joswiak et al., 2009). Fragment 9 (hereafter F9/T77; Fig. 2e) consists of a Cr- and Mn-rich pigeonite (transitional to augite; $En_{86}Wo_{10}$; Cr_2O_3 = 2.62 wt%; MnO = 7.95 wt%; Joswiak et al., 2012). Major element compositions of microtome sections of the T77 particles, which were measured using TOF-SIMS, were similar to those that we described above (Stephan, 2009).

3.2. A particle from track 22

Fragment 7 from track 22 (hereafter F7/T22; Fig. 2g) consists of FeO-rich olivine (Fo_{67-91}) and Al ± Na silicate glass. F7/T22 can be classified as a coarse-grained particle, because FeO-rich olivine and glass are larger than 1 μm. T22 exhibits a carrot-shape which tapers down towards the terminal particle (Joswiak et al., 2012) and can thus be classified as a type A track (Burchell et al., 2008).

3.3. A particle from track 57

Track 57 was classified as a type B track (Joswiak et al., 2012). Fragment 10 (hereafter F10/T57; Fig. 2h) consists of forsterite (Fo_{98}) and is enriched in MnO (1.30 wt%). Because the MnO/FeO ratio is < 1(FeO = 2.24 wt%), F10/T57 is not classified as a LIME olivine, but is considered a Mn-rich forsterite. Unlike F10/T57, the terminal particle of track 57 is composed of a large pyrrhotite crystal with attached fine-grained material consisting of sub-μm silicates and sulfides. These fragments, along with other fragments and material studied in the track indicate that the original projectile that produced track 57 was an aggregate of fine- and coarse-grained particles (Joswiak et al., 2012). NanoSIMS analyses of TEM sections of material adjacent to the terminal particle show nitrogen isotope anomalies ($\delta^{15}N$ from +420‰ to +640‰), which correspond to those of carbonaceous material (Matrajt et al., 2008).

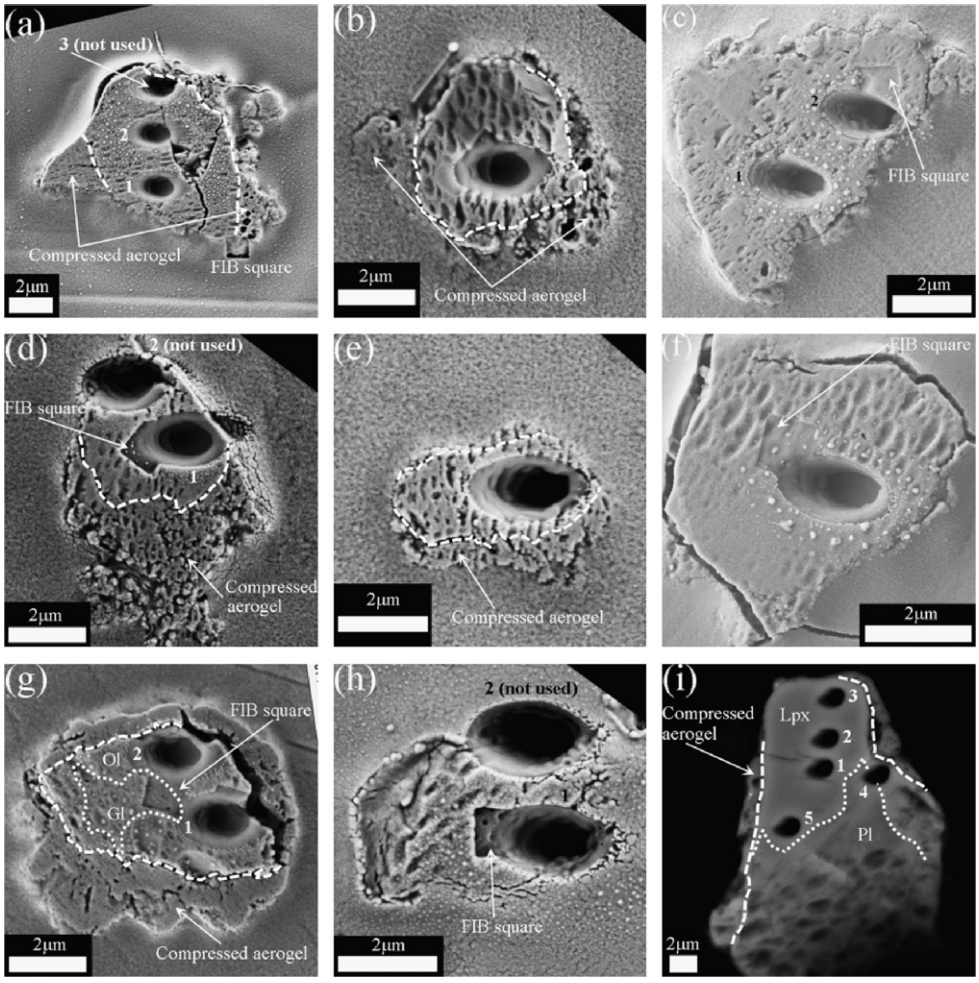

Fig. 2. SE and BSE images of the Wild 2 particles after oxygen isotope analyses; (a) F1/T77, (b) F4/T77, (c) F5/T77, (d) F6/T77, (e) F9/T77, (f) F50/T77, (g) F7/T22, (h) F10/T57, and (i) F1/T81 (BSE). Numbers near the SIMS pits in panels a, c, d, g, h, and i indicate spot numbers of SIMS analysis, which correspond to spot numbers in Table 1. Dashed lines correspond to boundary between Wild 2 particles and compressed aerogel. The dotted line in panel g corresponds to boundary between olivine (Ol) and Al + Na silicate glass (Gl), whereas that in panel i corresponds to boundaries between low-Ca pyroxene (Lpx) and plagioclase (Pl). White small spherical materials around the SIMS pits are Cs deposits. In panel i, the surface of plagioclase is partially dark and has numerous dimples. This is because the surface of F1/T81 is tilted against the polished surface and plagioclase is partially underneath epoxy, so that the dimples on the plagioclase surface made by microtoming were not removed during the polishing.

3.4. *A particle from track 81*

Track 81 is classified as a type B track (see http://www.curator.jsc.nasa.gov/stardust/catalog/index.cfm), from which fragment 1 was extracted (terminal particle; F1/T81; 15×20 μm). F1/T81 consists of low-Ca pyroxene ($En_{92}Wo_3$; $\sim 10 \times 10$ μm) and plagioclase ($An_{65}Ab_{35}$; $\sim 15 \times 15$ μm) (Fig. 2i) and is similar to TEM analyses obtained from microtomed thin sections of the same fragment as analyzed by Dobrică and Brearley (2011). Because the original microtomed surface of F1/T81 was slightly tilted against the polished epoxy surface (Fig. 2i) the surface of F1/T81 is partially underneath epoxy. However, the 10×10 μm surface area of low-Ca pyroxene that was exposed was large enough for multiple spot analyses by SIMS.

4. Results of oxygen isotope analyses

We made a total of nineteen spot analyses in nine Wild 2 particles. After inspection of the SIMS analysis spots by FE-SEM, 3 out of the 19 analyses were rejected, because they overlapped with the edge of the particle and surrounding aerogel and/or acrylic (spot 3 in F1/T77, spot 2 in F6/T77, and spot 2 in F10/T57; Fig. 2). A summary of the sixteen spot analyses taken from all 9 particles is shown in Table 1; a more complete table is given in the Supplementary Table A1. For samples with FIB-marks, the SIMS spots were located within 0.4 μm of the center of FIB-square on average (see the Supplementary information).

The oxygen isotope ratios show a wide variation from −50‰ to +7‰ in $\delta^{18}O$ along the Carbonaceous Chondrite Anhydrous Mineral (CCAM) and Young and Russell (Y&R) lines (Clayton et al., 1977; Young and Russell, 1998; Fig. 3). The data from three Mn-rich forsterite particles including two LIME olivine particles (F6/T77, F50/T77, and F10/T57) plot at the lower end of the CCAM line; their $\Delta^{17}O$ values are around −23‰ (Table 1). One of the three data points (spot 1 in F10/T57) deviates from the slope-1 lines towards low $\delta^{18}O$ (Fig. 3). This might be due to the ion beam hitting a small fraction of acrylic (see the Supplementary information; McKeegan et al., 2006). The effect of acrylic contamination, however, on the measured $\Delta^{17}O$ value is not significant (see the Supplementary information).

The other six particles show oxygen isotope ratios that plot around the TF line (F1/T77, F4/T77, F5/T77, F9/T77, F7/T22, and F1/T81), similar to Wild 2 particles from previous studies (Fig. 3; McKeegan et al., 2006; Nakamura et al., 2008; Nakashima et al., 2011a; Ogliore et al., 2012). Data from two FeO-poor particles

Table 1
Oxygen isotope ratios of the nine Wild 2 particles measured using the three-hole disk and IMS-1280.[a,b,c]

Track#	Sample name (NASA JSC name)	Spot#	$\delta^{18}O \pm 2SD$ (‰)		$\delta^{17}O \pm 2SD$ (‰)		$\Delta^{17}O \pm 2SD$ (‰)		Target[d]	Size (μm)
77	F1/T77 (C2009,20,77,1,0)	1	6.0	1.4	4.4	1.5	1.3	1.7	Fo_{65}	7 × 8
		2	5.3	1.4	4.1	1.5	1.3	1.7		
		Average					1.3	1.2		
77	F4/T77 (C2009,20,77,4,0)		6.8	1.8	2.1	1.4	−1.5	1.2	Fo_{60}	4 × 4
77	F5/T77 (C2009,20,77,5,0)	1	7.1	1.7	5.5	2.8	1.8	2.5	$En_{42}Wo_{46}$	5 × 7
		2	2.8	1.7	2.9	2.8	1.4	2.5	mixed[e]	
		Average					1.6	1.8		
77	F6/T77 (C2009,20,77,6,0)		−46.4	1.8	−47.0	1.4	−22.9	1.2	LIME Ol ($Fo_{99.8}$)	4 × 4
77	F9/T77 (C2009,20,77,9,0)		0.3	1.8	−2.9	1.4	−3.0	1.2	$En_{86}Wo_{10}$	2 × 4
77	F50/T77 (C2009,20,77,50,0)		−48.8	1.8	−49.2	1.8	−23.9	1.6	LIME Ol ($Fo_{99.8}$)	4 × 4
22	F7/T22 (C2115,24,22,7,0)	1	6.7	2.4	5.9	1.5	2.5	1.7	Fo_{79}	4 × 6
		2	2.5	2.4	0.6	1.5	−0.7	1.7		
57	F10/T57 (C2009,2,57,10,0)	1	−55.5	1.5	−50.9	1.0	−22.0	1.3	Fo_{98} (Mn−rich)	3 × 4
81	F1/T81 (C2092,7,81,1,0)	1	1.8	3.0	−0.2	1.7	−1.1	1.8	$En_{92}Wo_3$	15 × 20
		2	1.4	3.0	0.1	1.7	−0.6	1.8	$En_{92}Wo_3$	
		3	3.2	3.0	0.4	1.7	−1.3	1.8	$En_{92}Wo_3$	
		4	2.0	3.0	0.1	1.7	−0.9	1.8	$En_{92}Wo_3 + An_{65}Ab_{35}$	
		5	2.5	3.0	−0.5	1.7	−1.8	1.8	$En_{92}Wo_3$	
		Average	2.2	1.3	0.0	0.7	−1.1	0.8		

[a] The uncertainties associated with isotope ratios are external reproducibility (2SD) of eight sets of bracketing analyses of San Carlos olivine standard grains which are embedded with the Wild 2 particles in 8 mm disks.
[b] Instrumental bias correction was applied for all the spots. Average values of the chemical compositions were used for instrumental bias correction.
[c] The uncertainties associated with average values are twice the standard error of the mean (2SE).
[d] Average (or representative) chemical compositions are shown (Joswiak et al., 2012).
[e] Spot 2 in F5/T77 is a mixed phase between olivine (Fo_{66}) and diopside ($En_{42}Wo_{46}$) in the proportion of one part to 1.6, and may also include a glass phase, but which is not taken account.

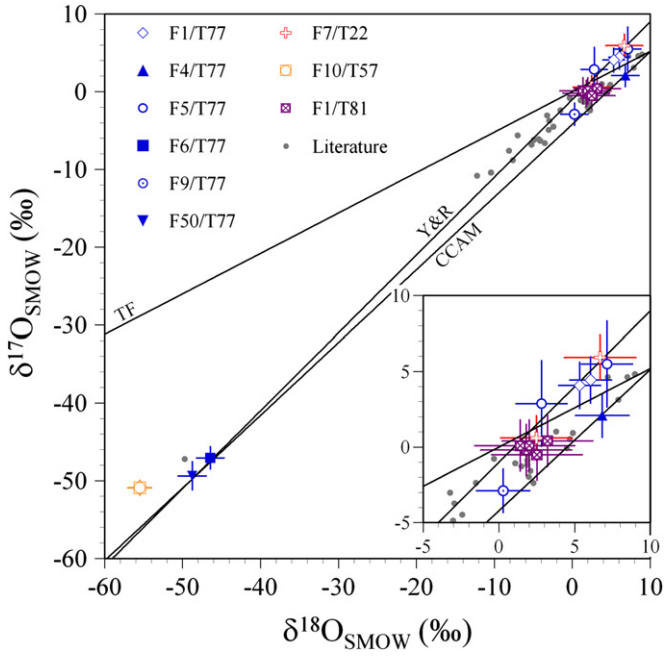

Fig. 3. Oxygen three-isotope ratios of the nine Wild 2 particles. TF, Y&R, and CCAM represent the terrestrial fractionation line, the Young and Russell line, and the carbonaceous chondrite anhydrous mineral line. Literature data of ferromagnesian Wild 2 particles are shown for comparison, which are from McKeegan et al. (2006), Nakamura et al. (2008), Nakashima et al. (2011a), and Ogliore et al. (2012).

(F9/T77 and F1/T81) plot below the TF line. Isotope ratios of F1/T81 are reproducible within analytical uncertainties, and the average and 2SE (standard error of the mean) of $\Delta^{17}O$ values of five analyses are -1.1 ± 0.8‰. Data from FeO-rich particles, excluding F4/T77 data and one of two data from F7/T22, plot above the TF line. The $\Delta^{17}O$ values from F7/T22 are −0.7‰ and +2.5‰ and marginally different (3.2 ± 2.3‰). We treat the two data from F7/T22 separately. While the $\Delta^{17}O$ values from F5/T77 are consistent within the analytical uncertainties (average value = $+1.6 \pm 1.8$‰; 2SE), the $\delta^{18}O$ values differ significantly (7.1‰ and 2.8‰; Table 1). Spot 2 of F5/T77 ($\delta^{18}O$ of 2.8‰) appears to have overlapped Al–Si-glass (67 wt% SiO_2; Joswiak et al., 2009), but the instrumental bias correction for a mixture of diopside and FeO-rich olivine was applied (Table 1). It is likely that the $\delta^{18}O$ and $\delta^{17}O$ values of Spot 2 are underestimated along the mass fractionation line because the instrumental bias (in $\delta^{18}O$) of SiO_2-rich glass is significantly lower than that of diopside and FeO-rich olivine by ~10‰ (Valley and Kita, 2009).

5. Discussion

5.1. Mn-rich forsterite Wild 2 particles with ^{16}O-rich oxygen isotope ratios

All three Mn-rich forsteritic Wild 2 particles have ^{16}O-rich oxygen isotope ratios ($\Delta^{17}O \sim -23$‰). Mn-rich forsterite, known as LIME olivine, was identified in IDPs (Klöck et al., 1989), amoeboid olivine aggregates (AOAs, e.g., Weisberg et al., 2004; Sugiura et al., 2009; Ruzicka et al., 2012), chondrules in CR chondrites (Ichikawa and Ikeda, 1995), and matrix of primitive chondrites such as Semarkona (LL3.0) and Murchison (CM; Klöck et al., 1989). Ebel et al. (2012) suggested that LIME olivine formed by condensation from a reduced vapor of solar composition (see also Klöck et al., 1989; Klöck and Stadermann, 1994). It is unlikely that Mn-rich forsteritic Wild 2 particles formed by reduction of FeO- and MnO-rich olivine because of the absence of detectable metallic iron inclusions as a product of reduction in the Mn-rich forsterite Wild 2 particles (Fig. 2d, f, h).

Weisberg et al. (2004) argued that the formation temperature of Mn-rich forsterite in the solar nebula was between 1100 K and 1440 K (see also Sugiura et al., 2009), corresponding to the condensation temperatures of Mn_2SiO_4 and Mg_2SiO_4,

respectively. These high temperatures should have been achieved only in the inner solar nebula. The $\Delta^{17}O$ values of $\sim -23‰$ for the three Mn-rich forsterite particles are similar to those of LIME olivines from AOAs ($\sim -20‰$) but different from that of LIME olivine from an anhydrous IDP ($\sim -2‰$) (e.g., Weisberg et al., 2007; Aléon et al., 2002, 2009). Similar to the CAI-like particle in Track 25 (Inti) (McKeegan et al., 2006), the Mn-rich forsterites might have been transported to comet assembly regions from the innermost solar nebula where ^{16}O-rich CAIs and AOAs might have formed ($\Delta^{17}O \sim -20‰$; Krot et al., 2002). Nakamura-Messenger et al. (2011) reported a similar ^{16}O-rich forsterite Wild 2 particle from track 112 ($\Delta^{17}O \sim -27‰$) and suggested that the particle formed by condensation from an ^{16}O-rich solar nebula gas together with refractory inclusions.

5.2. Oxygen isotope heterogeneity of particles from a single track

Six particles extracted from T77 have variable mineral compositions (Joswiak et al., 2012). The $\Delta^{17}O$ values scatter widely from $\sim -23‰$ to $+1.6‰$ and show a few ‰ variation from $-3.0 \pm 1.2‰$ to $+1.6 \pm 1.8‰$ (Table 1), which was not observed in previous studies of Wild 2 particles from single tracks (Nakamura et al., 2008; Nakamura-Messenger et al., 2011). Although an ^{16}O-rich relict olivine grain was found in the chondrule-like particle Gozen-sama, the Mg# of the relict olivine was consistent with other minerals in the same particle (Nakamura et al., 2008). The original projectile (>6 μm; Joswiak et al., 2009) that was captured in aerogel was an aggregate of μm to sub-μm size silicate particles that formed in a range of environments.

5.3. Comparison of $\Delta^{17}O$-Mg# trends between ferromagnesian Wild 2 particles and chondrules

Nakamura et al. (2008) discovered Wild 2 particles that were similar to chondrules in carbonaceous chondrites in terms of their mineralogy, igneous textures, and negative $\Delta^{17}O$ values. Due to the lack of heat sources to form chondrules in the Kuiper belt, they suggested that chondrule-like objects formed in asteroidal regions must have been later transported to comet assembly regions. Although annealing in the inner solar nebula, as suggested by Nuth et al. (2000), cannot be entirely ruled out, true igneous chondrule-forming processes may have been essential for producing the crystalline silicate particles in comet Wild 2 (e.g., Nakamura et al., 2008, 2009; Ogliore et al., 2012). Here we compare oxygen isotope systematics between ferromagnesian Wild 2 particles and chondrite chondrules, which may help to constrain the source of solid materials that were transported to the Kuiper belt.

In Fig. 4a, we plot $\Delta^{17}O$ values of ferromagnesian Wild 2 particles against their Mg# using results obtained in this study (six particles from Table 1) along with five additional Wild 2 particles from the literature (Nakamura et al., 2008; Nakashima et al., 2011a; Ogliore et al., 2012) with 1–2‰ precision (Table 2). The averages of multiple spot analyses are shown, except for F7/T22 which shows two different $\Delta^{17}O$ values. The 11 particles shown in Fig. 4a are derived from 8 different tracks. Data from a ^{16}O-rich relict olivine in Gozen-sama (Nakamura et al., 2008) and ^{16}O-rich forsterite (Nakamura-Messenger et al., 2011) are excluded. Five FeO-poor particles (Mg# >90) in Fig. 4a show indistinguishable $\Delta^{17}O$ values, with the average value of

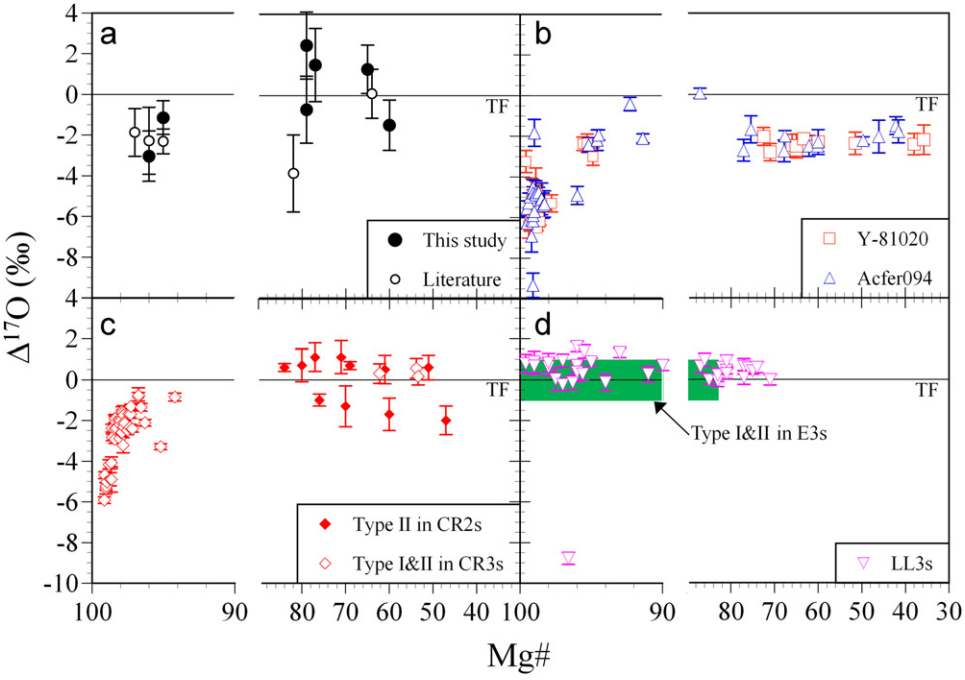

Fig. 4. Comparisons between $\Delta^{17}O$ values and Mg# of ferromagnesian Wild 2 particles, excluding ^{16}O-rich particles (a), chondrules from Acfer 094 and Yamato-81020 chondrites (b), chondrules from CR chondrites (c), and chondrules from LL3 and enstatite type 3 (E3) chondrites (d). Note the difference in the Mg# scaling between type I chondrules (FeO-poor particles) and type II chondrules (FeO-rich particles). Literature data of Wild 2 particles are from Nakamura et al. (2008), Nakashima et al. (2011a), and Ogliore et al. (2012). $\Delta^{17}O$ values and Mg# of carbonaceous chondrite chondrules are from Ushikubo et al. (2012) for Acfer 094 chondrules, Tenner et al. (2011a) for Yamato-81020 chondrules, Tenner et al. (2011b, 2012) and Connolly and Huss (2010) for CR chondrite chondrules, Kita et al. (2010) for LL3 chondrite chondrules, and Weisberg et al. (2011) for enstatite type 3 chondrite chondrules. In panel a, an enstatite particle from track 69 is not plotted, because the Mg# is not available (McKeegan et al., 2006). For a FeO-rich particle with $\Delta^{17}O$ of $-3.8‰$, uncertainty is 2SD. Data in panel c contain many data of type II chondrules which were selectively analyzed by Connolly and Huss (2010), though type II chondrules are much less common compared to type I chondrules in CR chondrites (Weisberg et al., 1995). The $\Delta^{17}O$ values increase with decreasing Mg# for Wild 2 particles and carbonaceous chondrite chondrules, but not for chondrules from LL3 chondrites and enstatite type 3 chondrites. The $\Delta^{17}O$–Mg# trend of the Wild 2 particles resembles CR chondrite chondrules most.

Table 2
Mg# and $\Delta^{17}O$ values of ferromagnesian crystalline silicate Wild 2 particles in the previous studies with 1–2‰ precision[a].

Track#	Sample name	Mg#	$\Delta^{17}O \pm 2SE$ (‰)		Remark	References
35	Torajiro[b]	82	−3.8	1.9	Chondrule-like	Nakamura et al. (2008)
69			−1.6	0.6	Enstatite	McKeegan et al. (2006)
74	Iris	64	−0.3	2	Chondrule-like	Ogliore et al. (2012)
108	Gozen-sama	95	−2.3	0.6	Chondrule-like	Nakamura et al. (2008)
108	Gen-chan	96	−2.3	1.7	Chondrule-like	Nakamura et al. (2008)
130	Bidi	97	−1.9	1.2	Ol+Hpx+Pl+SiO_2	Nakashima et al. (2011a); Joswiak et al. (2012).

[a] Mg# and $\Delta^{17}O$ values are average values excluding ^{16}O-rich relict grains. For average $\Delta^{17}O$ value of Torajiro, while Ushikubo et al. (2012) used only pyroxene data, we used all oxygen isotope data from olivine and pyroxene.
[b] Uncertainty of average $\Delta^{17}O$ value of Torajiro is 2SD.

-2.1 ± 1.3‰ (2SD, $n=6$, including an enstatite particle from track 69 without reported Mg#; McKeegan et al., 2006). The $\Delta^{17}O$ values of six FeO-rich particles (Mg#=60–82) range from −3.8‰ to +2.5‰. We note that the lowest $\Delta^{17}O$ value (−3.8‰) is from the FeO-rich particle Torajiro (track 35), which is reported to be internally heterogeneous (Nakamura et al., 2008). Except for Torajiro, the average $\Delta^{17}O$ value of the FeO-rich particles is $+0.1 \pm 3.0$‰ (2SD, $n=5$).

Chondrule data are compiled mainly from the recent high precision SIMS data of type ~3.0 chondrites with known Mg# of mafic minerals (Kita et al., 2010; Connolly and Huss, 2010; Tenner et al., 2011a, 2011b, 2012; Ushikubo et al., 2012), which are shown in Fig. 4b–d.

For Acfer 094 (an ungrouped type 3.0 carbonaceous chondrite) and Yamato-81020 (CO3.0), chondrules mainly show a bimodal distribution of $\Delta^{17}O$ at ~−5‰ and ~−2‰ for chondrules with Mg#>96 and <96 (including type II chondrules), respectively (Fig. 4b; Ushikubo et al., 2012; Tenner et al., 2011a). Rudraswami et al. (2011) observed similar results from the Allende CV3 chondrite (petrologic type >3.6; Bonal et al., 2006), though the $\Delta^{17}O$-Mg# trend is not shown due to possible changes of Mg# from thermal metamorphism. Chondrules and isolated olivines in Murchison (CM) studied by Jabeen and Hiyagon (2003) seem to show a bimodal distribution of $\Delta^{17}O$ very similar to that in Fig. 4b. The majority of chondrules in these chondrites are those with Mg# >96 and $\Delta^{17}O$ of ~−5‰.

In contrast, chondrules in CR chondrites frequently have $\Delta^{17}O$ values of ~−2‰ (Krot et al., 2006b) and show a different $\Delta^{17}O$–Mg# trend (Fig. 4c). The $\Delta^{17}O$ values of most type I chondrules (Mg# ≥90) cluster at −2‰ with most Mg-rich chondrules (Mg# ≥98) being systematically lower in $\Delta^{17}O$ down to −5‰ (Tenner et al., 2011b, 2012; see also Krot et al., 2006b), while those of type II chondrules distribute from −2‰ to +1‰ (Connolly and Huss, 2010; see also Schrader et al., 2012). CH and CH/CB chondrites contain abundant cryptocrystalline chondrules that show bimodal $\Delta^{17}O$ values of −2‰ and +1.5‰ for FeO-poor and FeO-rich ones, respectively, while those of porphyritic chondrules scatter widely from −5‰ to +5‰ (Krot et al., 2010; Nakashima et al., 2010, 2011b). Isolated olivine and pyroxene (most likely liberated chondrule phenocrysts) in CI chondrites show a systematic $\Delta^{17}O$ increase from ~−5‰ to +3‰ with decreasing Mg# from 99 to 70 (Leshin et al., 1997). The FeO-poor (Mg# ≥97) chondrules and olivine separates from Tagish Lake (C2-ungrouped) show the $\Delta^{17}O$ values from −5‰ to −2‰ that are inversely correlated to Mg# (Russell et al., 2010). These data are very similar to those of CR chondrites.

Unlike chondrules in carbonaceous chondrites, most chondrules from type 3 LL and enstatite chondrites show fairly constant $\Delta^{17}O$ values independent of Mg#: −0.2‰ to +1.6‰ and −1‰ to +1‰, respectively (Fig. 4d; Kita et al., 2010; Weisberg et al., 2011). The $\Delta^{17}O$ distributions of forsteritic olivines from carbonaceous and ordinary chondrites (Libourel and Chaussidon, 2011) are consistent with those shown in Fig. 4b–d.

The different distributions observed among chondrites may represent heterogeneous oxygen isotope reservoirs that existed in the protoplanetary disk (e.g., Ushikubo et al., 2012). Repeated chondrule formation processes accompanying evaporation and condensation of solid precursors would homogenize local isotope reservoirs (Kita et al., 2010; Ushikubo et al., 2012). For carbonaceous chondrite chondrules, the addition of water ice with $\Delta^{17}O$ >0‰ to the anhydrous solid precursors would result in systematic increase of $\Delta^{17}O$ values for type II chondrules compared to those of type I chondrules in the same chondrites (Fig. 4b–c; Connolly and Huss, 2010; Tenner et al., 2012; Ushikubo et al., 2012).

The $\Delta^{17}O$ values of the ferromagnesian Wild 2 particles range from −4‰ to +2.5‰ (Fig. 4a). In particular, the $\Delta^{17}O$ values of FeO-poor particles (Mg#=95–97) cluster at −2‰ and those of FeO-rich particles (Mg#=60–82) scatter mainly from −1.5‰ to +2.5‰. FeO-poor crystalline silicates with $\Delta^{17}O$ >0‰ and ~−5‰ have not been observed. Although the amount of data available is limited ($n=12$), the $\Delta^{17}O$–Mg# trend of the Wild 2 particles most closely resembles CR chondrite chondrules among the chondrite groups described above. This is in agreement with the suggestion from mineralogy and chemistry of Wild 2 particles and chondrites (Weisberg and Connolly, 2008) and late formation of many CR chondrules and type II chondrule-like Wild 2 particle Iris compared to chondrules in other chondrites based on ^{26}Al chronology (>3 Ma vs. ~2 Ma after CAIs; Nagashima et al., 2007, 2008; Hutcheon et al., 2009; Ogliore et al., 2012; see also Kita and Ushikubo, 2012). It should be noted that there are notable differences between chondrules in CR chondrites and Wild 2 particles. Phenocryst sizes in the chondrule-like Wild 2 particles (≤10 μm; Nakamura et al., 2008; Ogliore et al., 2012) are much smaller than those in CR chondrules (≥50 μm; Krot et al., 2006b; Connolly and Huss, 2010), which may be due to sampling bias for Wild 2 particles (Brownlee et al., 2012). It seems that FeO-rich particles are more frequently observed from comet Wild 2 crystalline silicates than in carbonaceous chondrites including CR chondrites (Zolensky et al., 2006, 2008; Dobrică et al., 2009). The FeO/MnO ratios of FeO-rich Wild 2 olivines overlap not only those in CR chondrites but also in other carbonaceous and ordinary chondrites (Frank et al., 2012). In spite of these differences, the similarity of the $\Delta^{17}O$–Mg# trends between chondrules in CR chondrites and ferromagnesian Wild 2 particles suggests a close relation between their local disk environments that had similar oxygen isotope ratios and redox states.

5.4. Implication to the origin of crystalline silicate Wild 2 particles

Oxygen isotope analyses revealed that crystalline silicates from comet Wild 2 include ^{16}O-rich and relatively ^{16}O-poor particles, which is very similar to primitive chondrites that contain ^{16}O-rich CAIs and relatively ^{16}O-poor chondrules (e.g., Yurimoto et al., 2008). It is suggested that both ^{16}O-rich and -poor solids were widely distributed throughout the outer solar nebula, from the asteroid belt to the Kuiper belt (Aléon et al., 2009;

Ushikubo et al., 2012). The ^{16}O-rich Mn-rich forsterite Wild 2 particles may have been transported from where ^{16}O-rich refractory inclusions formed (the innermost solar nebula) to comet-forming regions by outward flow in the protoplanetary disk, as the early formed refractory inclusions were widely dispersed in the solar nebula (e.g., Ciesla, 2010).

In contrast, chondrules show different characteristics for each chondrite group including oxygen isotope systematics (Fig. 4b–d) and size of chondrules (Scott and Krot, 2003; Jones, 2012). A similarity of oxygen isotope ratios between bulk chondrules and their host chondrites (e.g., Clayton, 2003) indicates that chondrite accretion regions may be closely related to chondrule formation regions, which might have been spatially separated for different chondrite groups (e.g., Kurahashi et al., 2008). Chondrules might have formed later than refractory inclusions (e.g., Kita and Ushikubo, 2012) in a dust-rich layer of the protoplanetary disk where efficiency of radial transport was low enough and they did not migrate far before they accreted to planetesimals. However, given the similarity of oxygen isotope systematics between crystalline silicate Wild 2 particles and CR chondrules, some fractions of crystalline silicates in comet Wild 2 were derived from the inner protoplanetary disk that may be closely related to the location of CR chondrite parent body formation.

Here we discuss a possible location of source regions of Wild 2 crystalline silicates in the early solar nebula. It is generally considered that accretion locations of carbonaceous chondrites were further from the Sun than those of enstatite and ordinary chondrites based on chondrite properties (e.g., Rubin and Wasson, 1995). Among carbonaceous chondrites, CR chondrites show large deuterium and ^{15}N enrichments in organics, H_2O, and bulk samples that may be the products of low temperature chemistry in the interstellar medium or the early outer Solar System (Weisberg et al., 1995; Busemann et al., 2006; Floss and Stadermann, 2009; Alexander et al., 2010), suggesting accretion of CR chondrites at the furthest locations of any carbonaceous chondrite (Fig. 5), probably outer regions of the asteroid belt. Alternatively, Aléon (2010) suggested that a late accretion of CR chondrites accounts for the ^{15}N enrichments. These two suggestions are compatible, given that the growth of an object is slower at larger heliocentric distances (cf., Weidenschilling, 2005). Thus, we suggest that both chondrules in CR chondrites and many crystalline silicates in Wild 2 formed in the furthest regions of chondrule formation. This is consistent with frequent occurrence of FeO-rich particles with $\Delta^{17}O > 0‰$ that may have formed by an addition of ^{16}O-poor water ice, given that further locations from the Sun may have been more abundant in water ice (e.g., Cuzzi and Zahnle, 2004). Crystalline silicates at greater heliocentric distances might have been transported outward more effectively, considering that the Sun's gravitational potential is inversely related to the heliocentric distance. Although particles from inner asteroid regions would have been transported to comet-forming regions, an appreciable fraction of the ferromagnesian crystalline silicates in comet Wild 2 might have been delivered from the furthest regions of chondrule formation, which probably corresponds to the outer regions of the asteroid belt.

6. Conclusions

Oxygen three-isotope ratios of nine Wild 2 particles were analyzed using a 1×2 μm spot with ± 0.4 μm aiming accuracy. Three Wild 2 particles of Mn-rich forsterite showed $\Delta^{17}O$ values of $\sim -23‰$, which are comparable to those of ^{16}O-rich AOAs and CAIs (e.g., Aléon et al., 2002). It is suggested that the three Mn-rich forsterite particles formed by condensation from an ^{16}O-rich gaseous reservoir in the innermost solar nebula.

Six particles from track 77, a type B track, showed a significantly large chemical and isotope heterogeneity with the $\Delta^{17}O$ variation from $-24‰$ to $+1.6‰$. The original projectile of the track 77 particles may have been an aggregate of silicate particles that formed in a range of environments.

Four FeO-rich Wild 2 particles showed $\Delta^{17}O$ values from $-1.5‰$ to $+2.5‰$, while two FeO-poor particles showed $\Delta^{17}O$ values of $-3.0‰$ and $-1.1‰$. Combined with results of the previous studies, the $\Delta^{17}O$ values of the ferromagnesian Wild 2 particles distribute from $-4‰$ to $+2.5‰$, while $\Delta^{17}O$ values of FeO-poor particles (Mg#=95–97) cluster at $-2‰$ and those of FeO-rich particles (Mg#=60–82) scatter mainly from $-1.5‰$ to $+2.5‰$. The $\Delta^{17}O$-Mg# trend is most similar to that of chondrules in CR chondrites, but very different from other carbonaceous chondrites, including Acfer 094, CO3, and CV3. Many of the crystalline silicate particles may have been derived from the outer regions of the asteroid belt where carbonaceous chondrites formed.

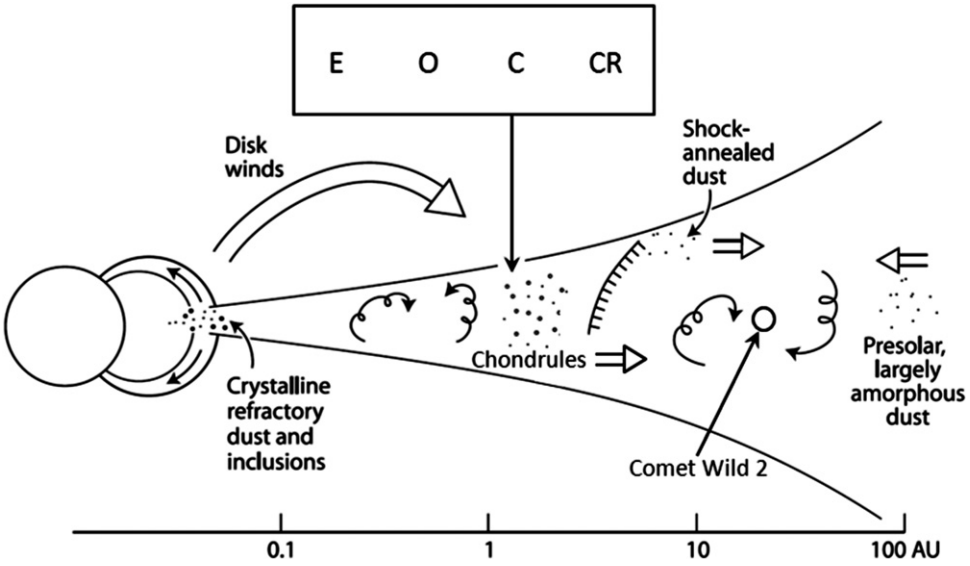

Fig. 5. Schematic diagram showing outward radial transport processes from the inner solar nebula to the comet assembly regions (Fig. 2 from Scott and Krot, 2005) Abbreviations: E, enstatite chondrites; O, ordinary chondrites; C, carbonaceous chondrites; CR, CR chondrites.

Acknowledgments

The manuscript was greatly improved by reviews from J. Aléon and an anonymous reviewer. The authors thank R.K. Noll for help with FIB and FE-SEM observation, H. Xu and P.E. Brown for use of a polarizing microscope and high magnification objective lens, J. Kern for SIMS support, and T.J. Tenner for kindly providing oxygen isotope data of CR3 chondrite chondrules and for discussion. R.C. Ogliore and K. Nagashima kindly provided us oxygen isotope data of the Wild 2 particle Iris for our discussion. This work is supported by various NASA programs (NK, NNX09AC30G; DB, NNX10AI89GS01; Cosmochemistry and Laboratory Analysis of Returned Samples Program to MZ). WiscSIMS is partly supported by NSF-EAR (0319230, 0744079, 1053466).

Appendix A. Supporting information

Supplementary data associated with this article can be found in the online version at http://dx.doi.org/10.1016/j.epsl.2012.09.041.

References

Aléon, J., 2010. Multiple origins of nitrogen isotopic anomalies in meteorites and comets. Astrophys. J. 722, 1342–1351.

Aléon, J., Krot, A.N., McKeegan, K.D., 2002. Calcium-aluminum-rich inclusions and amoeboid olivine aggregates from the CR carbonaceous chondrites. Meteorit. Planet. Sci. 37, 1729–1755.

Aléon, J., Engrand, C., Leshin, L.A., McKeegan, K.D., 2009. Oxygen isotopic composition of chondritic interplanetary dust particles: a genetic link between carbonaceous chondrites and comets. Geochim. Cosmochim. Acta 73, 4558–4575.

Alexander, C.M.O'D., Newsome, S.D., Fogel, M.L., Nittler, L.R., Busemann, H., Cody, G.D., 2010. Deuterium enrichments in chondritic macromolecular material-Implications for the origin and evolution of organics, water and asteroids. Geochim. Cosmochim. Acta 74, 4417–4437.

Bonal, L., Quirico, E., Bourot-Denise, M., Montagnac, G., 2006. Determination of the petrologic type of CV3 chondrites by Raman spectroscopy of included organic matter. Geochim. Cosmochim. Acta 70, 1849–1863.

Bradley, J.P., 2003. Interplanetary dust particles. In: Davis, A.M. (Ed.), Treatise in Geochemistry. Elsevier-Pergamon, pp. 689–711.

Bridges, J.C., Changela, H.G., Nayakshin, S., Starkey, N.A., Franchi, I.A., 2012. Chondrule fragments from Comet Wild2: evidence for high temperature processing in the outer solar system. Earth Planet. Sci. Lett. 341–344, 186–194.

Brownlee, D., Tsou, P., Aleon, J., Alexander, C.M.O., Araki, T., Bajt, S., Baratta, G.A., Bastien, R., Bland, P., Bleuet, P., Borg, J., Bradley, J.P., Brearley, A., Brenker, F., Brennan, S., Bridges, J.C., Browning, N.D., Brucato, J.R., Bullock, E., Burchell, M.J., Busemann, H., Butterworth, A., Chaussidon, M., Cheuvront, A., Chi, M., Cintala, M.J., Clark, B.C., Clemett, S.J., Cody, G., Colangeli, L., Cooper, G., Cordier, P., Daghlian, C., Dai, Z., D'hendecourt, L., Djouadi, Z., Dominguez, G., Duxbury, T., Dworkin, J.P., Ebel, D.S., Economou, T.E., Fakra, S., Fairey, S.A.J., Fallon, S., Ferrini, G., Ferroir, T., Fleckenstein, H., Floss, C., Flynn, G., Franchi, I.A., Fries, M., Gainsforth, Z., Gallien, J.-P., Genge, M., Gilles, M.K., Gillet, P., Gilmour, J., Glavin, D.P., Gounelle, M., Grady, M.M., Graham, G.A., Grant, P.G., Green, S.F., Grossemy, F., Grossman, L., Grossman, J.N., Guan, Y., Hagiya, K., Harvey, R., Heck, P., Herzog, G.F., Hoppe, P., Horz, F., Huth, J., Hutcheon, I.D., Ignatyev, K., Ishii, H., Ito, M., Jacob, D., Jacobsen, C., Jacobsen, S., Jones, S., Joswiak, D., Jurewicz, A., Kearsley, A.T., Keller, L.P., Khodja, H., Kilcoyne, A.D., Kissel, J., Krot, A., Langenhorst, F., Lanzirotti, A., Le, L., Leshin, L.A., Leitner, J., Lemelle, L., Leroux, H., Liu, M.-C., Luening, K., Lyon, I., Macpherson, G., Marcus, M.A., Marhas, K., Marty, B., Matrajt, G., Mckeegan, K., Meibom, A., Mennella, V., Messenger, K., Messenger, S., Mikouchi, T., Mostefaoui, S., Nakamura, T., Nakano, T., Newville, M., Nittler, L.R., Ohnishi, I., Ohsumi, K., Okudaira, K., Papanastassiou, D.A., Palma, R., Palumbo, M.E., Pepin, R.O., Perkins, D., Perronnet, M., Pianetta, P., Rao, W., Rietmeijer, F.J.M., Robert, F., Rost, D., Rotundi, A., Ryan, R., Sandford, S.A., Schwandt, C.S., See, T.H., Schlutter, D., Sheffield-Parker, J., Simionovici, A., Simon, S., Sitnitsky, I., Snead, C.J., Spencer, M.K., Stadermann, F.J., Steele, A., Stephan, T., Stroud, R., Susini, J., Sutton, S.R., Suzuki, Y., Taheri, M., Taylor, S., Teslich, N., Tomeoka, K., Tomioka, N., Toppani, A., Trigo-Rodriguez, J.M., Troadec, D., Tsuchiyama, A., Tuzzolino, A.J., Tyliszczak, T., Uesugi, K., Velbel, M., Vellenga, J., Vicenzi, E., Vincze, L., Warren, J., Weber, I., Weisberg, M., Westphal, A.J., Wirick, S., Wooden, D., Wopenka, B., Wozniakiewicz, P., Wright, I., Yabuta, H., Yano, H., Young, E.D., Zare, R.N., Zega, T., Ziegler, K., Zimmerman, L., Zinner, E., Zolensky, M., 2006. Comet 81P/Wild 2 under a microscope. Science 314, 1711–1716.

Brownlee, D.E., Joswiak, D.J., Matrajt, G., 2012. Overview of the rocky component of Wild 2 comet samples: insight into the early solar system, relationship with meteoritic materials and differences between comets and asteroids. Meteorit. Planet. Sci. 47, 453–470.

Burchell, M.J., Fairrey, S.A.J., Wozniakiewicz, P., Brownlee, D.E., Hörz, F., Kearsley, A.T., See, T.H., Tsou, P., Westphal, A., Green, S.F., Trigo-Rodríguez, J.M., Domingúez, G., 2008. Characteristics of cometary dust tracks in Stardust aerogel and laboratory calibrations. Meteorit. Planet. Sci. 43, 23–40.

Busemann, H., Young, A.F., Alexander, C.M.O'D., Hoppe, P., Mukhopadhyay, S., Nittler, L.R., 2006. Interstellar chemistry recorded in organic matter from primitive meteorites. Science 312, 727–730.

Busemann, H., Nguyen, A.N., Cody, G.D., Hoppe, P., Kilcoyne, A.L.D., Stroud, R.M., Zega, T.J., Nittler, L.R., 2009. Ultra-primitive interplanetary dust particles from the comet 26P/Grigg-Skjellerup dust stream collection. Earth Planet. Sci. Lett. 288, 44–57.

Ciesla, F.J., 2007. Outward transport of high-temperature materials around the midplane of the solar nebula. Science 318, 613–615.

Ciesla, F.J., 2010. The distributions and ages of refractory objects in the solar nebula. Icarus 208, 455–467.

Clayton, R.N., 2003. Oxygen isotopes in meteorites. In: Davis, A.M. (Ed.), Meteorites, Comets, and Planets, Treatise on Geochemistry, vol. 1. Elsevier B V, Amsterdam, pp. 129–142.

Clayton, R.N., Onuma, N., Grossman, L., Mayeda, T.K., 1977. Distribution of the pre-solar component in Allende and other carbonaceous chondrites. Earth Planet. Sci. Lett. 34, 209–224.

Connolly Jr., H.C, Huss, G.R., 2010. Compositional evolution of the protoplanetary disk: oxygen isotopes of type-II chondrules from CR2 chondrites. Geochim. Cosmochim. Acta 74, 2473–2483.

Cuzzi, J.N., Zahnle, K.J., 2004. Material enhancement in protoplanetary nebulae by particle drift through evaporation front. Astrophys. J. 614, 490–496.

Dobrică, E., Engrand, C., Duprat, J., Gounelle, M., Leroux, H., Quirico, E., Rouzaud, J.-N., 2009. Connection between micrometeorites and Wild 2 particles: from Antarctic snow to cometary ices. Meteorit. Planet. Sci. 44, 1643–1661.

Dobrică, E., Brearley, A.J., 2011. Crystalline silicates in comet 81P/Wild 2 from the stardust track 81. Meteorit. Planet. Sci. 46, A59. (abstr.).

Ebel, D.S., Weisberg, M.K., Beckett, J.R., 2012. Thermochemical stability of low-iron, manganese-enriched olivine in astrophysical environments. Meteorit. Planet. Sci. 47, 585–593.

Floss, C., Stadermann, F.J., 2009. High abundances of circumstellar and interstellar C-anomalous phases in the primitive CR3 chondrites QUE 99177 and MET 00426. Astrophys. J. 697, 1242–1255.

Floss, C., Stadermann, F.J., Bradley, J.P., Dai, Z.R., Bajt, S., Graham, G., Lea, A.S., 2006. Identification of isotopically primitive interplanetary dust particles: a NanoSIMS isotopic imaging study. Geochim. Cosmochim. Acta 70, 2371–2399.

Frank, D.R., Zolensky, M.E., Le, L., 2012. Using the Fe/Mn ratio of FeO-rich olivine in Wild 2, chondrite matrix, and type IIA chondrules to disentangle their histories. Lunar Planet. Sci., XLIII (#2748).

Gounelle, M., Morbidelli, A., Bland, P.A., Sephton, M.A., Young, E.D., Spurny, P., 2008. Meteorites from the outer solar system? In: Barucci, A., Boehnhardt, H., Cruikshank, D., Morbidelli, A. (Eds.), The Solar System Beyond Neptune. Arizona University Press, Tucson, pp. 525–541.

Heck, P.R., Ushikubo, T., Schmitz, B., Kita, N.T., Spicuzza, M.J., Valley, J.W., 2010. A single asteroidal source for extraterrestrial Ordovician chromite grains from Sweden and China: high-precision oxygen three-isotope SIMS analysis. Geochim. Cosmochim. Acta 74, 497–509.

Hutcheon, I.D., Marhas, K.K., Krot, A.N., Goswami, J.N., Jones, R.H., 2009. ^{26}Al in plagioclase-rich chondrules in carbonaceous chondrites: evidence for an extended duration of chondrule formation. Geochim. Cosmochim. Acta 73, 5080–5099.

Ichikawa, O., Ikeda, Y., 1995. Petrology of the Yamato-8449 CR chondrite. Proceedings of the NIPR Symposium on Antarctic Meteorites 8, 63–78.

Ishii, H.A., Bradley, J.P., Dai, Z.R., Chi, M., Kearsley, A.T., Burchell, M.J., Browning, N.D., Molster, F., 2008. Comparison of comet 81P/Wild 2 dust with interplanetary dust from comets. Science 319, 447–450.

Ishii, H.A., Stadermann, F.J., Floss, C., Joswiak, D., Bradley, J.P., Teslich, N., Brownlee, D.E., Matrajt, G., MacPherson, G., McKeegan, K.D., 2010. Lack of evidence for in situ decay of aluminum-26 in comet 81P/Wild 2 CAI-like refractory particles 'Inti' and 'Coki'. Lunar Planet. Sci. XLI, 2317. (abstr.).

Jabeen, I., Hiyagon, H., 2003. Oxygen isotopes in isolated and chondrule olivines from Murchison. Lunar Planet. Sci. XXXIV, 1551. (abstr.).

Jones, R.H., 2012. Petrographic constraints on the diversity of chondrule reservoirs in the protoplanetary disk. Meteorit. Planet. Sci. 47, 1176–1190.

Joswiak, D.J., Brownlee, D.E., Matrajt, G., Westphal, A.J., Snead, C.J., 2009. Kosmochloric Ca-rich pyroxenes and FeO-rich olivines (Kool grains) and associated phases in Stardust tracks and chondritic porous interplanetary dust particles: possible precursors to FeO-rich type II chondrules in ordinary chondrites. Meteorit. Planet. Sci. 44, 1561–1588.

Joswiak, D.J., Brownlee, D.E., Matrajt, G., Westphal, A.J., Snead, C.J., Gainsforth, Z., 2012. Comprehensive examination of large mineral and rock fragments in Stardust tracks: mineralogy, analogous extraterrestrial materials and source regions. Meteorit. Planet. Sci. 47, 471–524.

Kita, N.T., Ushikubo, T., 2012. Evolution of protoplanetary disk inferred from ^{26}Al chronology of individual chondrules. Meteorit. Planet. Sci 47, 1108–1119.

Kita, N.T., Ushikubo, T., Fu, B., Valley, J.W., 2009. High precision SIMS oxygen isotope analysis and the effect of sample topography. Chem. Geol. 264, 43–57.

Kita, N.T., Nagahara, H., Tachibana, S., Tomomura, S., Spicuzza, M.J., Fournelle, J.H., Valley, J.W., 2010. High precision SIMS oxygen three isotope study of chondrules in LL3 chondrites: role of ambient gas during chondrule formation. Geochim. Cosmochim. Acta 74, 6610–6635.

Klöck, W., Stadermann, F.J., 1994. Mineralogical and chemical relationships of interplanetary dust particles, micrometeorites and meteorites. Analysis of Interplanetary Dust. In: Zolensky, E., Wilson, T.L., Rietmeijer, F.J.M., Flynn, G.J. Proceedings of the NASA/LPI Workshop held in Houston, TX, May 1993. New York, American Institute of Physics Press. AIP Conference Proceedings, vol. 310, p. 51.

Klöck, W., Thomas, K.L., McKay, D.S., Palme, H., 1989. Unusual olivine and pyroxene composition in interplanetary dust and unequilibrated ordinary chondrites. Nature 339, 126–128.

Krot, A.N., McKeegan, K.D., Leshin, L.A., MacPherson, G.J., Scott, E.R.D., 2002. Existence of an ^{16}O-rich gaseous reservoir in the solar nebula. Science 295, 1051–1054.

Krot, A.N., Yurimoto, H., McKeegan, K.D., Leshin, L., Chaussidon, M., Libourel, G., Yoshitake, M., Huss, G.R., Guan, Y., Zanda, B., 2006a. Oxygen isotopic compositions of chondrules: implications for evolution of oxygen isotopic reservoirs in the inner solar nebula. Chem. der Erde 66, 249–276.

Krot, A.N., Libourel, G., Chaussidon, M., 2006b. Oxygen isotope compositions of chondrules in CR chondrites. Geochim. Cosmochim. Acta 70, 767–779.

Krot, A.N., Nagashima, K., Yoshitake, M., Yurimoto, H., 2010. Oxygen isotopic compositions of chondrules from the metal-rich chondrites Isheyevo (CH/CB$_b$), MAC 02675 (CB$_b$) and QUE 94627 (CB$_b$). Geochim. Cosmochim. Acta 74, 2190–2211.

Kurahashi, E., Kita, N.T., Nagahara, H., Morishita, Y., 2008. ^{26}Al-^{26}Mg systematics of chondrules in a primitive CO chondrite. Geochim. Cosmochim. Acta 72, 3865–3883.

Leitner, J., Heck, P.R., Hoppe, P., Huth, J. 2012. The C-, N-, and O-isotopic composition of cometary dust from comet 81P/Wild 2. Lunar Planet. Sci. XLIII, 1839. (abstr.).

Leshin, L.A., Rubin, A.E., McKeegan, K.D., 1997. The oxygen isotopic composition of olivine and pyroxene from CI chondrites. Geochim. Cosmochim. Acta 61, 835–845.

Libourel, G., Chaussidon, M., 2011. Oxygen isotopic constraints on the origin of Mg-rich olivines from chondritic meteorites. Earth Planet. Sci. Lett. 301, 9–21.

Lodders, K., Osborne, R., 1999. Perspectives on the comet–asteroid–meteorite link. Space Sci. Rev. 90, 289–297.

Matrajt, G., Ito, M., Wirick, S., Messenger, S., Brownlee, D.E., Joswiak, D.J., Flynn, G., Sandford, S., Snead, C., Westphal, A., 2008. Carbon investigation of two Stardust particles: a TEM, NanoSIMS, and XANES study. Meteorit. Planet. Sci. 43, 315–334.

McKeegan, K.D., Aléon, J., Bradley, J., Brownlee, D., Busemann, H., Butterworth, A., Chaussidon, M., Fallon, S., Floss, C., Gilmour, J., Gounelle, M., Graham, G., Guan, Y., Heck, P.R., Hoppe, P., Hutcheon, I.D., Huth, J., Ishii, H., Ito, M., Jacobsen, S.B., Kearsley, A., Leshin, L.A., Liu, M.-C., Lyon, I., Marhas, K., Marty, B., Matrajt, G., Meibom, A., Messenger, S., Mostefaoui, S., Mukhopadhyay, S., Nakamura-Messenger, K., Nittler, L., Palma, R., Pepin, R.O., Papanastassiou, D.A., Robert, F., Schlutter, D., Snead, C.J., Stadermann, F.J., Stroud, R., Tsou, P., Westphal, A., Young, E.D., Ziegler, K., Zimmermann, L., Zinner, E., 2006. Isotopic compositions of cometary matter returned by Stardust. Science 314, 1724–1728.

Messenger, S., Joswiak, D.J., Ito, M., Matrajt, G., Brownlee, D.E., 2009. Discoverry of presolar SiC from comet Wild-2. Lunar Planet. Sci. XL, 1790. (abstr.).

Nagashima, K., Krot, A.N., Chaussidon, M., 2007. Aluminum–magnesium isotope systematics of chondrules from CR chondrites. Meteorit. Planet. Sci 42, A115. (abstr.).

Nagashima, K., Krot, A.N., Huss, G.R., 2008. ^{26}Al in chondrules from CR carbonaceous chondrites. Lunar Planet. Sci. XXXXI, 2224. (abstr.).

Nakamura, T., Noguchi, T., Tsuchiyama, A., Ushikubo, T., Kita, N.T., Valley, J.W., Zolensky, M.E., Kakazu, Y., Sakamoto, K., Mashio, E., Uesugi, K., Nakano, T., 2008. Chondrulelike objects in short-period comet 81P/Wild 2. Science 321, 1664–1667.

Nakamura, T., Noguchi, T., Tsuchiyama, A., Ushikubo, T., Kita, N.T., Valley, J.W., Takahata, N., Sano, Y., Zolensky, M.E., Kakazu, Y., Uesugi, K., Nakano, T., 2009. Additional evidence for the presence of chondrules in Comet 81P/Wild 2. Meteorit. Planet. Sci. 44, A153. (abstr.).

Nakamura-Messenger, K., Keller, L.P., Clemett, S.J., Messenger, S., Ito, M., 2011. Nanometer-scale anatomy of entire Stardust tracks. Meteorit. Planet. Sci. 46, 1033–1051.

Nakashima, D., Kimura, M., Yamada, K., Noguchi, T., Ushikubo, T., Kita, N.T., 2010. Study of chondrules in CH chondrites—I: oxygen isotope ratios of chondrules. Meteorit. Planet. Sci. 45, A148. (abstr.).

Nakashima, D., Ushikubo, T., Zolensky, M.E., Weisberg, M.K., Joswiak, D.J., Brownlee, D.E., Matrajt, G., Kita, N.T., 2011a. High precision oxygen three isotope analysis of Wild 2 particles and anhydrous chondritic interplanetary dust particles. Lunar Planet. Sci. XLII, 1240. (abstr.).

Nakashima, D., Ushikubo, T., Rudraswami, N.G., Kita, N.T., Valley, J.W., Nagao, K., 2011b. Ion microprobe analyses of oxygen three-isotope ratios of chondrules from the Sayh al Uhaymir 290 chondrite using a multiple-hole disk. Meteorit. Planet. Sci. 46, 857–874.

Nakashima, D., Ushikubo, T., Zolensky, M.E., Kita, N.T., 2012. High precision oxygen three-isotope analyses of anhydrous chondritic interplanetary dust particles. Meteorit. Planet. Sci. 47, 197–208.

Nuth, J.A., Hill, H.G.M., Kletetschka, G., 2000. Determining the ages of comets from the fraction of crystalline dust. Nature 406, 275–276.

Ogliore, R.C., Huss, G.R., Nagashima, K., Butterworth, A.L., Gainsforth, Z., Stodolna, J., Westphal, A.J., Joswiak, D., Tyliszczak, T., 2012. Incorporation of a late-forming chondrule into comet Wild 2. Astrophys. J. 745, L19.

Rubin, A.E., Wasson, J.T., 1995. Variations of chondrite properties with heliocentric distance. Meteoritics 30, A569. (abstr.).

Rudraswami, N.G., Ushikubo, T., Nakashima, D., Kita, N.T., 2011. Oxygen isotope systematics of chondrules in Allende CV3 chondrite: high precision ion microprobe studies. Geochim. Cosmochim. Acta 75, 7596–7611.

Russell, S.D.J., Longstaffe, F.J., King, P.L., Larson, T.E., 2010. The oxygen-isotope composition of chondrules and isolated forsterite and olivine grains from the Tagish Lake carbonaceous chondrite. Geochim. Cosmochim. Acta 74, 2428–2499.

Ruzicka, A., Floss, C., Hutson, M., 2012. Amoeboid olivine aggregates (AOAs) in the Efremovka, Leoville and Vigarano (CV3) chondrites: a record of condensate evolution in the solar nebula. Geochim. Cosmochim. Acta 79, 79–105.

Schrader, D.L., Connolly Jr, H.C, Lauretta, D.S., Nagashima, K., Huss, G.R., Davidson, J., Domanik, K.J., 2012. O-isotope composition of the gas present during chondrule formation as recorded in CR chondrites. Lunar Planet. Sci. XLIII, 1627. (abstr.).

Scott, E.R.D., Krot, A.N., 2003. Chondrites and their components. In: Davis, A.M. (Ed.), Meteorites, Comets, And Planets, Treatise on Geochemistry, vol. 1. Elsevier.B V, Amsterdam, pp. 143–200.

Scott, E.R.D., Krot, A.N., 2005. Thermal processing of silicate dust in the solar nebula: clues from primitive chondrite matrices. Astrophys. J. 623, 571–578.

Stephan, T., 2009. TOF-SIMS analysis of cometary fragments extracted from a Stardust aerogel track. Lunar Planet. Sci. XL, 1698. (abstr.).

Stodolna, J., Gainsforth, Z., Butterworth, A., Westphal, A.J., 2012. TEM/STXM characterization of preserved primitive material from the comet Wild 2. Lunar Planet. Sci. XLIII, 1214. (abstr.).

Sugiura, N., Petaev, M.I., Kimura, M., Miyazaki, A., Hiyagon, H., 2009. Nebular history of amoeboid olivine aggregates. Meteorit. Planet. Sci 44, 559–572.

Tenner, T.J., Ushikubo, T., Kurahashi, E., Kita, N.T., Nagahara, H., 2011a. Oxygen isotopic measurements of phenocrysts in chondrules from the primitive carbonaceous chondrite Yamato 81020: evidence for two distinct oxygen isotope reservoirs. Lunar Planet. Sci. XLII, 1426. (abstr.).

Tenner, T.J., Nakashima, D., Ushikubo, T., Kita, N.T., Weisberg, M.K., 2011b. Oxygen isotope ratios in chondrules from primitive CR chondrite MET 00426: a correlation with chondrule Mg#. Meteorit. Planet. Sci. 46, A233. (abstr.).

Tenner, T.J., Nakashima, D., Ushikubo, T., Kita, N.T., Weisberg, M.K., 2012. Oxygen isotope ratios of chondrules from the Queen Alexandra Range 99177 (QUE 99177) CR3 chondrite: systematic relationships between chondrule Mg# and Δ^{17}O. Lunar Planet. Sci. XLIII, 2127. (abstr.).

Ushikubo, T., Kimura, M., Kita, N.T., Valley, J.W., 2012. Primordial oxygen isotope reservoirs of the solar nebula recorded in chondrules in Acfer 094 carbonaceous chondrite. Geochim. Cosmochim. Acta 90, 242–264.

Valley, J.W., Kita, N.T., 2009. In situ oxygen isotope geochemistry by ion microprobe. In; Mineralogical Association of Canada Short Course, vol. 41. Toronto, pp. 19–63.

Weidenschilling, S.J., 2005. Formation of the cores of the outer planets. Space Sci. Rev. 116, 53–66.

Weisberg, M.K., Connolly Jr, H.C, 2008. On the relationship between chondrites, comets and asteroids, a petrologic perspective. Lunar Planet. Sci. XXXIX, 1981. (abstr.).

Weisberg, M.K., Prinz, M., Clayton, R.N., Mayeda, T.K., Grady, M.M., Pillinger, C.T., 1995. The CR chondrite clan. Antarct. Meteorites 8, 11–32.

Weisberg, M.K., Connolly Jr., H.C, Ebel, D.S., 2004. Petrology and origin of amoeboid olivine aggregates in CR chondrites. Meteorit. Planet. Sci. 39, 1741–1753.

Weisberg, M.K., Kita, N.T., Ushikubo, T., Connolly Jr., H.C, Ebel, D.S., Spicuzza, M.J., Valley, J.W., 2007. Petrologic-isotopic study of amoeboid olivine aggregates in CR chondrites. Lunar Planet. Sci, XXXVIII, 1588. (abstr.).

Weisberg, M.K., Ebel, D.S., Connolly Jr., H.C., Kita, N.T., Ushikubo, T., 2011. Petrology and oxygen isotope compositions of chondrules in E3 chondrites. Geochim. Cosmochim. Acta 75, 6556–6569.

Young, E.D., Russell, S.S., 1998. Oxygen reservoirs in the early solar nebula inferred from an Allende CAI. Science 282, 452–455.

Yurimoto, H., Krot, A.N., Choi, B.-G., Aléon, J., Kunihiro, T., Brearley, A.J., 2008. Oxygen isotopes of chondritic components. In: MacPherson, G.J. (Ed.), Oxygen in The Solar System, Reviews in Mineralogy and Geochemistry, vol. 68. Mineralogical Society of America, Washington, D.C., pp. 141–186.

Zolensky, M.E., Zega, T.J., Yano, H., Wirick, S., Westphal, A.J., Weisberg, M.K., Weber, I., Warren, J.L., Velbel, M.A., Tsuchiyama, A., Tsou, P., Toppani, A., Tomioka, N., Tomeoka, K., Teslich, N., Taheri, M., Susini, J., Stroud, R., Stephan, T., Stadermann, F.J., Snead, C.J., Simon, S.B., Simionovici, A., See, T.H., Robert, F., Rietmeijer, F.J.M., Rao, W., Perronnet, M.C., Papanastassiou, D.A., Okudaira, K., Ohsumi, K., Ohnishi, I., Nakamura-Messenger, K., Nakamura, T., Mostefaoui, S., Mikouchi, T., Meibom, A., Matrajt, G., Marcus, M.A., Leroux, H., Lemelle, L., Le, L., Lanzirotti, A., Langenhorst, F., Krot, A.N., Keller, L.P., Kearsley, A.T., Joswiak, D., Jacob, D., Ishii, H., Harvey, R., Hagiya, K., Grossman, L., Grossman, J.N., Graham, G.A., Gounelle, M., Gillet, P., Genge, M.J., Flynn, G., Ferroir, T., Fallon, S., Ebel, D.S., Dai, Z.R., Cordier, P., Clark, B., Chi, M., Butterworth, A.L., Brownlee, D.E., Bridges, J.C., Brennan, S., Brearley, A., Bradley, J.P., Bleuet, P., Bland, P.A., Bastien, R., 2006. Mineralogy and petrology of Comet 81P/Wild 2 nucleus samples. Science 314, 1735–1739.

Zolensky, M., Nakamura-Messenger, K., Rietmeijer, F., Leroux, H., Mikouchi, T., Ohsumi, K., Simon, S., Grossman, L., Stephan, T., Weisberg, M., Velbel, M., Zega, T., Stroud, R., Tomeoka, K., Ohnishi, I., Tomioka, N., Nakamura, T., Matrajt, G., Joswiak, D., Brownlee, D., Langenhorst, F., Krot, A., Kearsley, A., Ishii, H., Graham, G., Dai, Z.R., Chi, M., Bradley, J., Hagiya, K.M., Gounelle, L., Keller Bridges, J, 2008. Comparing Wild 2 particles to chondrites and IDPs. Meteorit. Planet. Sci. 43, 261–272.